GLASS FINING EXPERIMENTS IN ZERO GRAVITY

H. D. Smith
Principal Investigator

D. M. Mattox
Program Manager

W. R. Wilcox and R. S. Subramanian
Consultants, Clarkson College of Technology

Final Report
Contract No. NAS8-32351
December 10, 1976 - June 30, 1977

June 30, 1977

George C. Marshall Space Flight Center
Marshall Space Flight Center, Alabama 35812

Westinghouse R&D Center
1310 Beulah Road
Pittsburgh, Pennsylvania 15235

GLASS FINING EXPERIMENTS IN ZERO GRAVITY

H. D. Smith
Principal Investigator

D. M. Mattox
Program Manager

W. R. Wilcox and R. S. Subramanian
Consultants, Clarkson College of Technology

Final Report
Contract No. NAS8-32351
December 10, 1976 - June 30, 1977

June 30, 1977

George C. Marshall Space Flight Center
Marshall Space Flight Center, Alabama 35812

Westinghouse R&D Center
1310 Beulah Road
Pittsburgh, Pennsylvania 15235

ABSTRACT

There is considerable interest in producing new and improved glasses in space by taking advantage of containerless processing. However, without gravity-induced movement of gas bubbles, considerable problems with bubbles are anticipated. One method suggested for fining (bubble removal) is to apply a temperature gradient, so as to cause the bubbles to move out because of the dependence of surface tension on temperature. Surface tension driven migration of bubbles in a thermal gradient has not been demonstrated previously in molten glasses. To provide the scientific basis for studying this effect in space, ground based experiments were conducted to demonstrate that thermal migration actually operated in glass melts. Thermal migration consistent with the theory was found in one experiment on a borax melt, i.e., there was an approximately linear relation between the bubble diameter and bubble velocity for a given temperature and temperature gradient. It also appeared that nearby bubbles were attracted to one another, which could greatly aid fining. Interpretation of these results was not possible because of complications arising from gravity, i.e., floating of the bubbles, circulation currents due to buoyancy-driven natural connection, and flow of the melt out from the cell.

TABLE OF CONTENTS

1. INTRODUCTION

There is one feature common to all aspects of glass melting: At one stage or another, raw materials are reacted which either liberate gases chemically combined or absorbed in the raw materials and/or entrap these gases (p cking voids) in the melting mixture. This leads to bubble entrapment. To render the glass transparent and to provide usable strength levels, these bubbles are eliminated in a process known as "fining." While this particular terminology is limited to bulk glasses, the requirement for eliminating bubbles is a dominant feature of the processing of most glass-containing systems. Ceramic-to-metal seals (high pressure sodium lamps) and glass-to-glass or glass-to-ceramic seals (cathode ray tubes) are formed with powdered glass (solder) seals. Hermeticity and acceptable strength directly correlate with the elimination of the void structure. Predictability and reliability in integrated circuits are commonly ensured by the use of passivating glass coatings. These are applied by elaborate techniques using powdered glass in liquid slurries to assure thin continuous coatings. The typical low expansion semiconducting materials require glasses which barely fuse at temperatures close to the stability limits of some of the components. The necessity of eliminating the entrapped bubbles dictates the times required at these elevated temperatures.

Another example of glass processing which is regulated by the bubble removal process is conventional porcelain enameling. In this process, bubbles must be eliminated to the point of leaving a smooth glassy surface. Surprisingly, in this particular application a rather well defined bubble structure imparts desirable performance benefits. In fact, certain additives, such as clay, are introduced to generate a bubble structure. The prevention of the defect called "fishscale" in sheet iron is one such benefit.

1.1 Buoyant Fining

In spite of the great wealth of experience possessed by glass manufacturers, little is understood about the process of fining and even less is understood about bubble elimination in sealing glasses or enamels. The traditional viewpoint[1-2] of glass fining is based on the effect of additives, called "fining agents." These decompose rapidly, to form new bubbles, or the gases diffuse into existing bubbles, causing them to grow, whereupon they rise quickly out of the melt under the action of buoyant forces. The velocity at which bubbles rise in the molten glass may be approximated by the following equation:

$$V = \frac{D^2 g \rho}{12\eta} \qquad (1)$$

where D = bubble diameter

g = gravitational constant

ρ = density of the melt

η = viscosity of the glass.

The factor 12 represents a departure from the typical Stokes formula because of the nonrigidity of the bubble.[3]

Simple calculation shows that beneath a particular size bubble, buoyant fining does not occur fast enough to eliminate bubbles in the times used in conventional processing. For example, a bubble 0.1 mm in diameter in a lime glass with a viscosity of 100 p will rise about 17 cm/day — too slow for commercial processing. An additional mechanism is necessary to explain the fining of commercial glasses.

1.2 "Chemical" Fining

One mechanism for the fining of commercial glasses has been elucidated by Greene and Gaffney.[4] Bubbles consisting largely of oxygen shrink until they disappear or reach a limiting size associated with the fraction of impurity gas originally present in the bubble. Doremus[5] proposes that the mechanism of fining agents such as As_2O_5 is to decrease the concentration of oxygen physically dissolved in the glass and permit

greater diffusion of oxygen out of the bubbles and into the glass. Carbon dioxide is also able to diffuse out of bubbles into the glass.[6] The function of most fining agents can be explained, then, in terms of making more oxygen available for diffusion (nitrates), or raising the diffusion coefficient of oxygen in the bulk melt (As_2O_5). These mechanisms might be called "chemical" fining.

1.3 "Thermal" Fining

"Thermal" fining, to coin a parallel phrase, is a mechanism that has been largely overlooked and little understood.[7] Temperature differences, with their effect on surface tension, produce a displacive force on bubbles, Thermal fining may be the principal mechanism of bubble elimination in sealing, soldering, and enamelling operations. It is commonly observed that bubbles come to the surface of glass enamel quickly regardless of the orientation of the enamel. Since seals, solders, and enamels are typically heated externally, it is presumed that a driving force toward the external surface is established on the bubbles in the fluid glass.

While significant evidence has been reported[8-12] which confirms that gas bubbles can move in a temperature gradient, no evidence has been reported for this phenomenon in glass systems, in spite of its obvious importance in glass sealing and enamelling. The effect of this mechanism has possibly been observed in experiences with direct electric melting of bulk glasses. Contrary to fuel fired furnaces, electric melters are hottest at the bottom of the tank. This gradient would oppose buoyant fining, and indeed, electrically melted glasses are harder to fine, although there are other factors which contribute to this.

While the mechanism of thermal fining is obviously of great commercial significance in many high technology applications, it represents an even more important mechanism in the space processing of glasses. There has been considerable interest in producing glasses in a zero gravity environment, particularly because the materials could be

produced without the use of a container and its unavoidable contamination. In the various equipment schemes proposed to date, no means have been proposed for eliminating the bubbles incorporated or exsolved as reboil during melting. If artificial gravitational fields were used they would nullify the potential benefits of zero G to some of the experiments, such as studies of the homogeneous nucleation of crystallizing glasses. Migration of bubbles under a temperature gradient could indeed serve as a fining mechanism in zero G for the production of bubble-free melts.

There is a need, therefore, for having a quantitative understanding of the migration of bubbles under a thermal gradient for both the control and understanding of 'art-laden' commercial processes and for application as a fining mechanism for zero G processing. This experiment definition study was therefore concerned with defining and developing a scientific basis which would justify experimentation in a low G environment and establish the flight hardware requirements. Specifically, unambiguous evidence for the migration of gas bubbles through a molten glass under the driving force of a thermal gradient was sought. The experiments were designed to reduce the influence of competitive mechanisms for movement, including surface tension driven convection. A prototype hot stage was developed which pointed toward a design which would be suitable for flight. The background and results of these experiments follow along with an evaluation and a proposal for flight experimentation.

2. EXPERIMENTAL BACKGROUND

2.1 Preparation of Candidate Glasses

The initial set of glasses considered for this experiment is listed in Table I, with their composition and batch materials. These glasses were mixed in 100 g batches, ball milled 1 hour, and melted in alumina crucibles. Each glass was melted several times to determine the lowest temperature capable of producing a reasonably well-refined glass. Since lead glasses or glasses with high alkali borate contents are volatile, a low melting temperature was desirable to remain close to the nominal composition and to prevent chemical inhomogeneities due to surface volatilization. It was found that glass batches B, C, and H melted to good glass with the least difficulty. They were melted at 800°C for 30 minutes. Glass I was melted at 900°C for 2 hours. Glass I was selected because it was a non-lead glass. These glasses were stored in cullet form (chunks) until needed for further experimentation.

Further preparation of these glasses consisted of crushing and sizing or remelting to introduce bubbles. Once crushed and sized the fractions were stored in glass bottles.

Remelted glass was stirred to introduce bubbles and then drawn up quartz capillary tubing or hand-drawn into glass cane, so as to produce a bubble array for one of the experimental techniques discussed later.

2.2 Design and Construction of Hot Stage Prototype

The prototype hot stage is pictured in Fig. 1. The heart of the stage is the tapered platinum strip held in position by the two copper terminal blocks. Small chromel-alumel thermocouples were spot welded to the bottom of the strip, allowing the temperature profile

TABLE I

Batch Compositions for Candidate Glasses

Glass A	88g PbO*	Glass G	60g PbO
	21.4g H_3BO_3		35.6g H_3BO_3
B	85g PbO		17.1g Na_2CO_3
	13.4g H_3BO_3		10g Al_2O_3
	7.5g SiO_2	H	79g PbO
C	85g PbO		19.6g H_3BO_3
	15g SiO_2		8g SiO_2
D	70g PbO		2g Al_2O_3
	26.7g H_3BO_3	I	36g SiO_2
	15g SiO_2		53g Na_2CO_3
E	75g PbO		24g TiO_2
	17.8g H_3BO_3		12.4g Li_2CO_3
	10g Al_2O_3		7.1g H_3BO_3
	5g SiO_2		
F	70g PbO		
	26.7g H_3BO_3		
	15g Al_2O_3		

*The following chemicals were used:

PbO - Fisher L-71
H_3BO_3 - Fisher L-73
SiO_2 - Stnd. Cer. Sup. - S925 (-200 mesh)
Al_2O_3 - Fisher A-591
Na_2CO_3 - Fisher S-263
TiO_2 - Fisher T-315
Li_2CO_3 - Fisher L-119

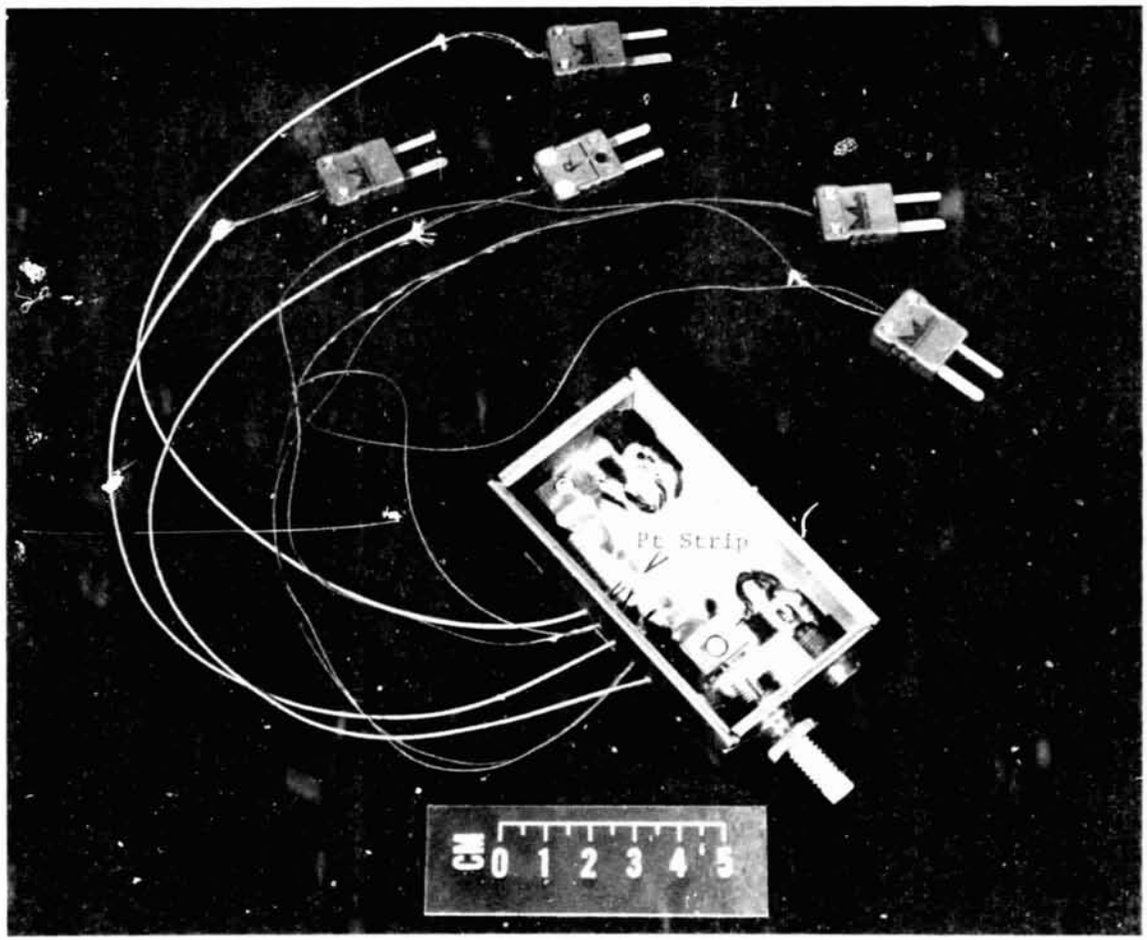

Fig. 1 - Prototype hot stage with platinum heating strip in place. Five thermocouples have been spot welded to the base of the strip. Spring tension mechanism prevents warping of the strip during heat up. Quartz cover glass not in place.

established by the strip to be determined. Banana plugs connected the stage to the power supply and were connected to the copper terminal blocks through flexible copper cables. The terminal blocks were mounted on a transite base with nylon screws. The sides were brass, fastened to the transite base. A simple spring tension mechanism maintained a flat configuration of the platinum strip as it heated, thus compensating for expansion. The copper terminal block to which it was attached had a split base which allowed it to slide freely back and forth in a track, while maintaining good electrical contact.

This stage fit easily on a research microscope sample stage. A quartz window fit on the ledge protecting the objective lens from high temperature and volatiles emenating from the hot glass. A 4X objective lens with a working distance of 7 mm or more easily focussed on the platinum strip surface.

For the preliminary screening experiments a simple strip profile has been used as seen in Fig. 1. This gave an adequate, but nonlinear, temperature gradient. R. S. Subramanian of Clarkson College has made an analysis of the thermal gradients in the heating strip. He has determined the equation which gives the width of the strip, Y_1, as a function of axial distance, X, necessary to establish a linear temperature gradient $(T_2-T_1)/L$ down the axis of the strip. The equation is:

$$Y_1^2(X) = \frac{I^2\rho_1}{4bL^2\sigma T_1^4} \quad \frac{1+\beta X}{(1+\alpha X)^4} \qquad (2)$$

where I = the current through the strip

ρ_1 = the electrical resistance of platinum at T_1

b = the thickness of the platinum strip

L = the length of strip for desired thermal gradient

σ = Stefan-Boltzmann constant

T_1 = temperature at the low temperature end of gradient

T_2 = temperature at the low temperature end of gradient

and $\beta = \frac{\rho_2-\rho_1}{\rho_1}$, $\alpha = \frac{T_2-T_1}{T_1}$ with ρ_2, T_2 equal to the resistance

and temperature of the platinum at the high temperature end of the linear thermal gradient. Here Y(X) and X are y(x)/L and x/L, the actual dimensions divided by L the length of the linear thermal gradient. Figure 2 illustrates how this linear gradient region is incorporated into the overall strip. The development of this equation is presented in Appendix A, along with the physical conditions assumed.

2.3 Preliminary Screening Experiments

The preliminary screening experiments allowed for familiarization with the operation of the hot stage as well as for observing the behavior of a molten layer of glass on the platinum strip. It was desired to observe the molten layer of glass because there were three types of instability that could develop due to horizontal and vertical temperature gradients energizing surface tension and buoyant forces. As described below, two kinds of cellular convection can be caused by a vertical temperature gradient. Whether or not they occur depends on the value of the Marangoni number for surface tension and the Raleigh number for buoyancy. As indicated by Subramanian's estimate of these numbers in Appendix B, they were far below the critical value for the molten glass film and, hence, should not have occurred.

A significant surface tension driven circulation was expected from the horizontal temperature gradient. As derived by Subramanian in Appendix C, the maximum rate of fluid flow at the free surface would be:

$$U_{max} = d/4\mu \quad d\gamma/d\chi \qquad (3)$$

where d = film thickness (cm)

μ = viscosity (dyne-sec/cm^2)

$d\gamma/d\chi$ = horizontal gradient of surface tension (dynes/cm^2). If the bubble is 1/10 the film thickness, then it is an order of magnitude larger and in the opposite direction expected for bubble motion, which is estimated to be:

$$v_b = - D_b/4\mu \quad d\gamma/d\chi$$

where D_b is the bubble diameter.

Dwg. 6403A57

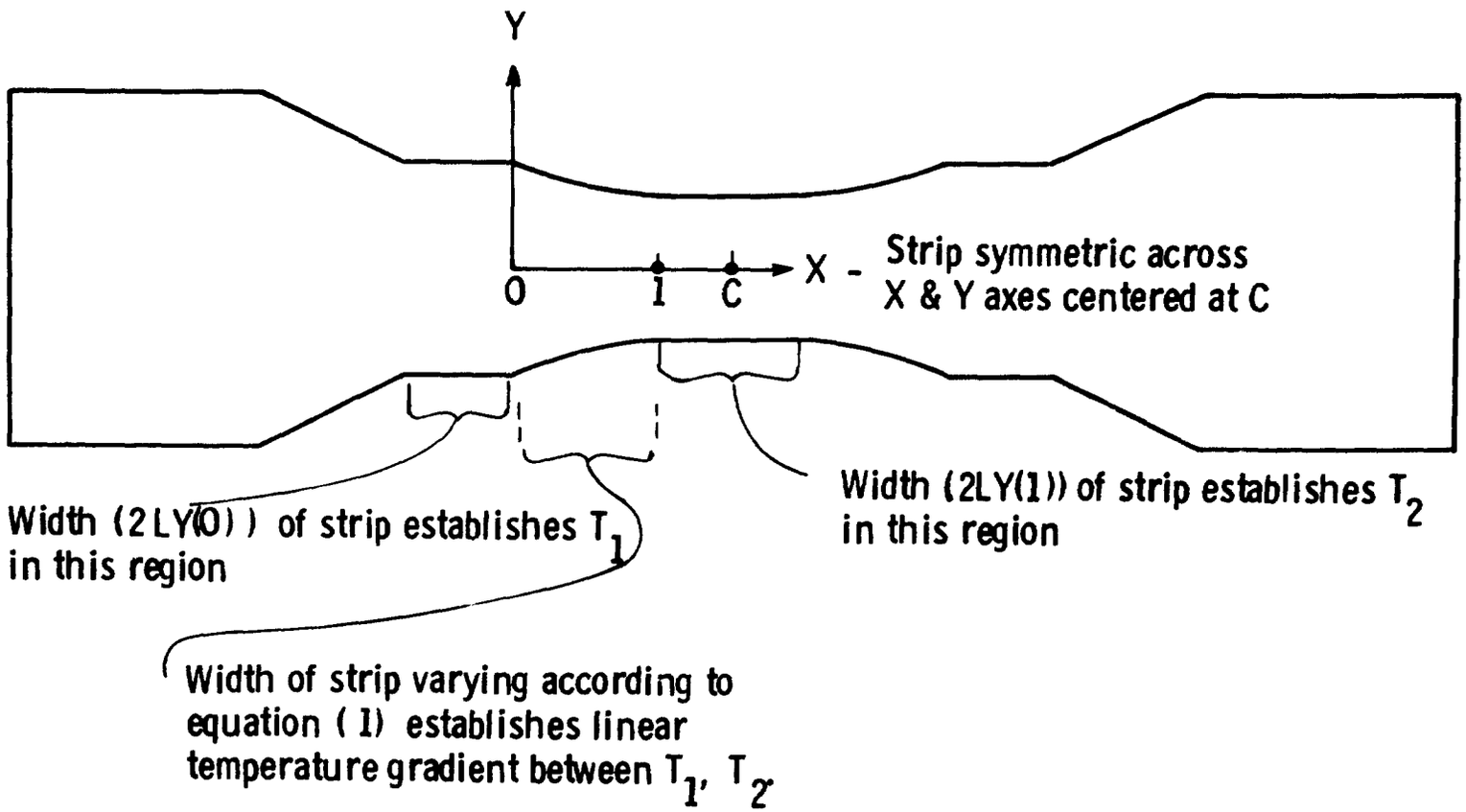

Fig. 2 — Schematic of platinum heating strip for hot stage

The resultant bubble motion would be very erratic and the bubble motion due to a thermal gradient almost impossible to measure.

Preliminary observation using fine zirconia as a tracer showed that the surface tension flow due to the horizontal gradient was indeed active and would probably swamp the effect we wanted to observe. This experimental confirmation led us to the modifications described in the next section.

2.4 Experimental Modifications and General Procedure

The surface tension phenomenon described above was avoided by eliminating all free surfaces. Two methods were found to be successful. The first and most successful was through the use of an inverted channel in a quartz window. This method, illustrated in Fig. 3, essentially isolated the bulk of the glass from the small amount of free surface remaining. For the inverted channel experiments the glass was pulled by hand to make cane ~1 mm in diameter. A section of cane, with the inverted channel in the quartz window over it, was placed on the platinum strip. The strip was heated, melting the glass cane which in a few minutes wetted the quartz, flowed into the channel, filled it, and established a film of glass everywhere between the platinum and the quartz window. Physical equilibrium was considered to be established when the meniscus at the ends of the channel stopped moving. Though considerable thermal migration must have gone on during this equilibration period, there were still many bubbles present. By raising the power to the strip, the motion was intensified (by both increasing the temperature gradient and lowering the viscosity).

The other method used a glass-filled quartz capillary 1 mm in diameter. Both eliminated all such surface tension driven flow of the bulk melt. The experimental procedure in each case was as follows. The glass to be used was melted, but not fined. If the bubble density was not high enough, bubbles were introduced by crude stirring. For

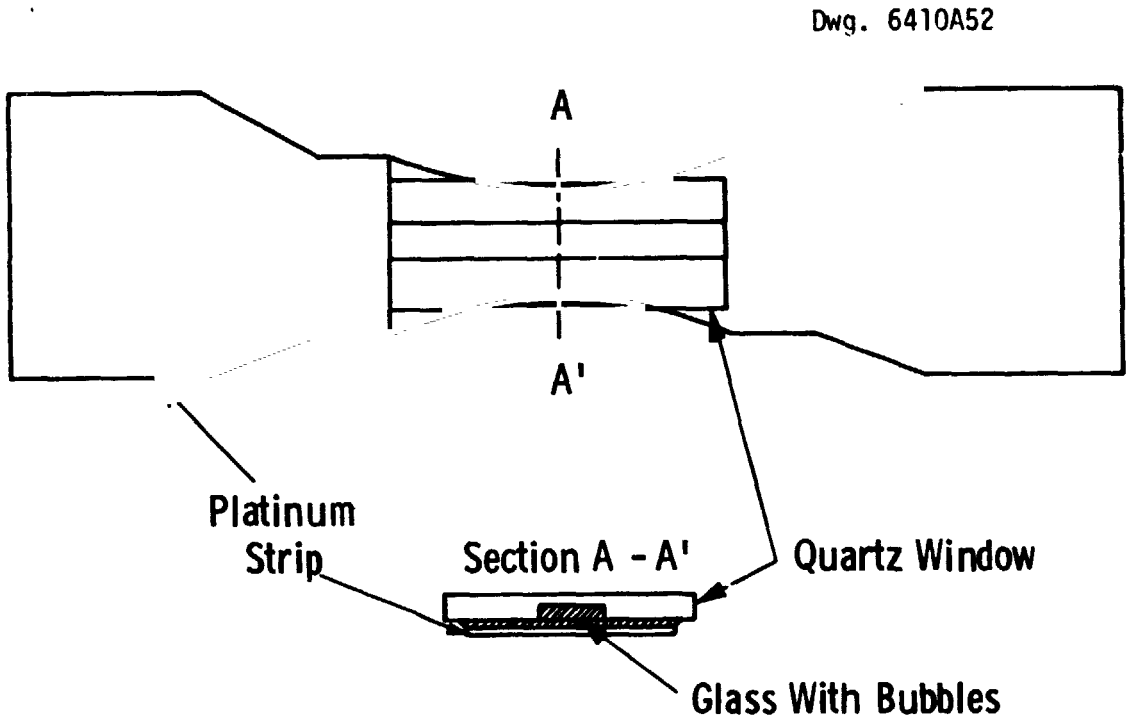

Fig. 3 – Quartz window with inverted channel

the capillary tube experiment, this glass was sucked into quartz capillary tubing which was subsequently broken into lengths to fit on the hot stage. The experiment consisted of placing the tube on the stage and heating enough to melt the entire length of glass. (If the entire length of glass was not melted the internal pressure in the capillary caused the bubbles to collapse and disappear.) Because of irreproducibility, it was found to be necessary to improve the thermal contact between the capillary and the heating strip by filling the area between the strip and the capillary with glass.

The inverted channel gave the best experimental results on the hot stage for several reasons. First, the heat transfer from the strip to the glass, which was in intimate contact with it, was much better than with a quartz capillary laying on the flat heating strip. Also, the small vertical dimension in the channel design allowed almost the entire depth to be viewed at one time. This made it much easier to follow bubble motion, because the competing buoyancy and surface tension effects caused bubbles to also move up and down. With the capillary this vertical movement often caused the bubbles to go in and out of focus. From the observable hot spot on the strip and the activity of the bubbles, it was also apparent that the gradient imposed on the strip was much more faithfully impressed on the molten glass with the inverted channel than with the quartz capillary. In fact, bubble motion didn't occur with the quartz capillary unless the capillary was "stuck" to the heating strip with an intermediate layer of molten glass, and then motion occurred as the capillary system "saw" the thermal gradient.

2.5 Temperature Response and Thermal Equilibration of the Hot Stage

The thermal response of the hot stage was measured using an IRCON infrared pyrometer. For these measurements, no attempt was made to correct for the emissivity of the platinum strip, thus all temperatures were relative. The measured long-term response is shown in Fig. 4, while the immediate response and that due to convection around the strip are not indicated.

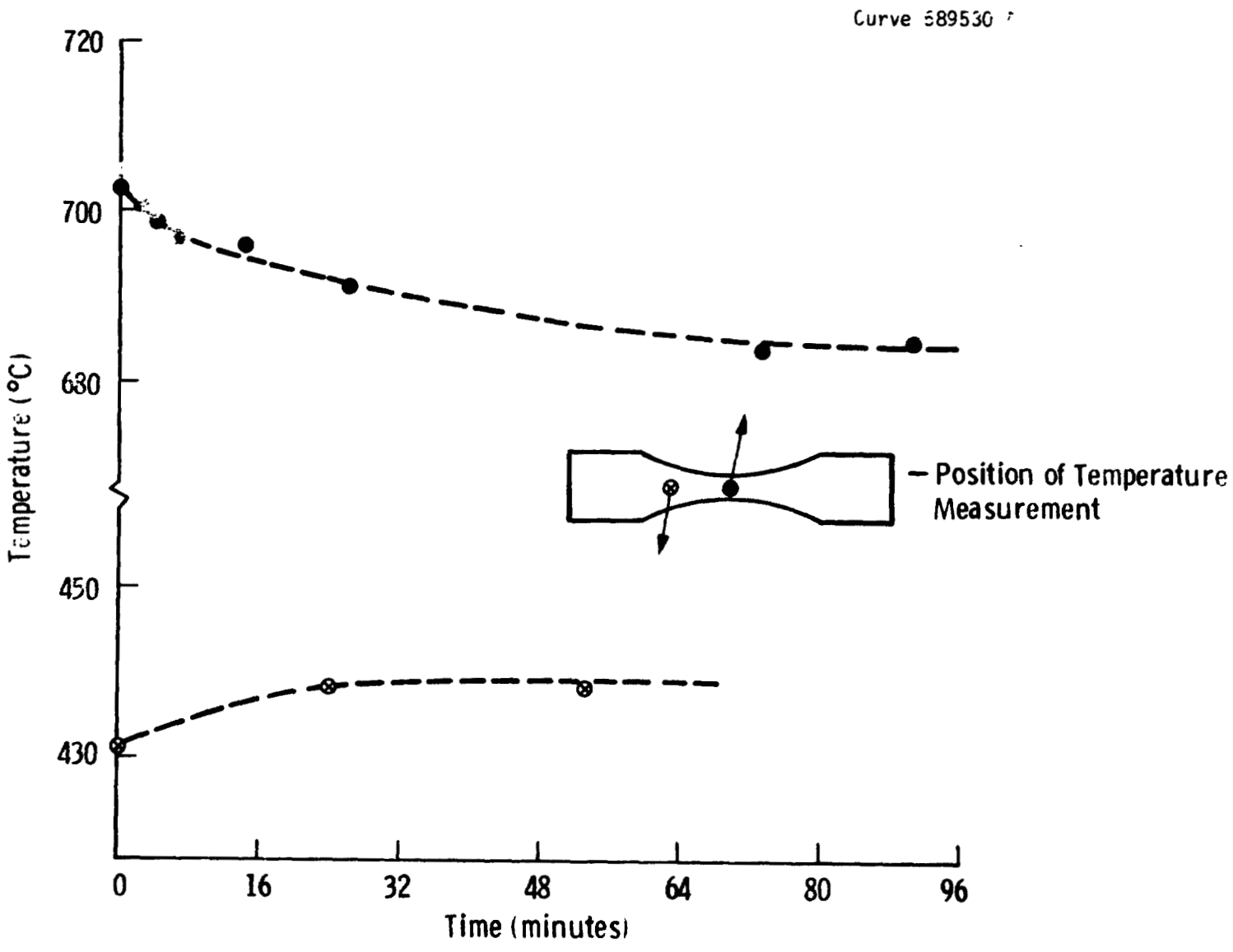

Fig. 4 – Temperature equilibration of hot stage. Measurements made with an infrared pyrometer on spots indicated

The first response of the hot stage was to heat quickly, within a few seconds after power was supplied to the initial temperature shown in Fig. 4. After this the temperature drifted slowly up to about 50°C. This drift is thought to have been caused by air circulation and/or free convection. Enclosing the platinum strip by putting on the glass cover almost completely eliminated this drift. The long-term response shown in Fig. 4 was a slight cooling of the "hot spot" on the platinum strip and heating of peripheral areas. This much slower response reflects the much lower heating rates in the periphery. As they heat slowly, more power is dissipated there and less in the "hot spot". The result is to cool the "hot spot" and increase the temperature of the cooler areas as shown.

2.6 Typical Temperature Profiles

As indicated previously, a design equation to enable establishment of a linear gradient was derived. To cut a platinum strip with the precision needed, it would have been necessary to use a flexible die. Since the system (and therefore the temperature and the gradient that was best to use) was not yet established, a carefully profiled heating strip was not used in these screening experiments. The alternative used was a simple tapered design like that indicated in Fig. 1. This produced a hot spot and a steep temperature gradient in both directions toward the copper posts. Thermocouples were spot welded to the underside of this platinum strip and from these the temperature profiles shown in Fig. 5 were determined. The highest temperature profile in Fig. 5 is the type used in our bubble migration experiments. Unfortunately the strips with thermocouples welded to them were too badly warped to be used successfully for the actual experiments. It is from this measured profile and others that we estimated (conservatively) the 300°C/cm gradient that is used for the calculations in Section 3.

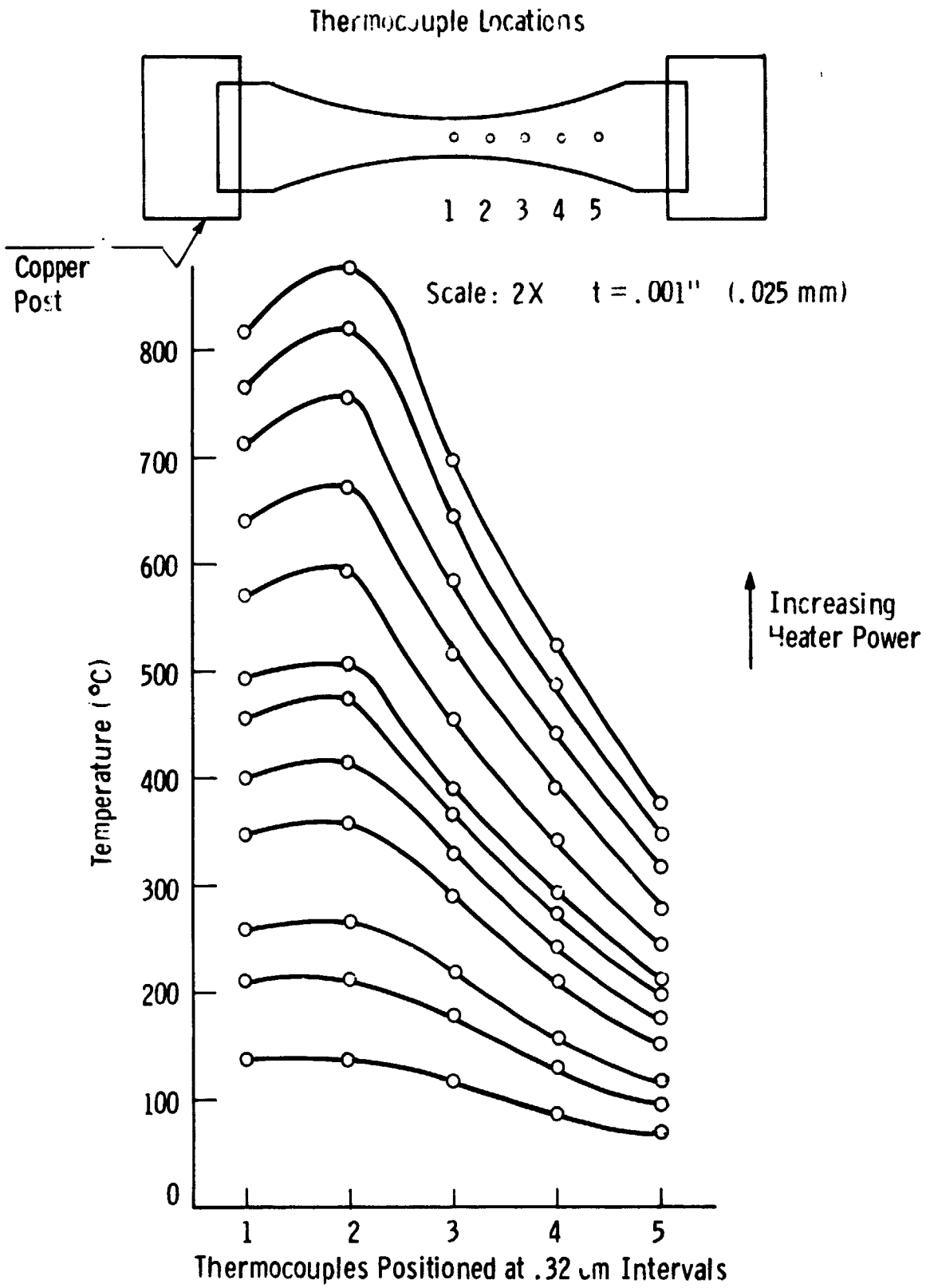

Fig. 5 – Measured temperature profiled for platinum strip shown in figure 1

3. RESULTS AND DISCUSSION

3.1 Thermal Migration in Common Lead Glasses

It is generally assumed that the surface tension of a liquid always decreases with increasing temperature.[13] With this assumption in mind, the glasses B, C, H, and J, were used for the initial bubble migration experiments. The negative (migration toward lower temperatures) and/or contradictory results obtained using these glasses was puzzling. Surface contamination or some other experimental problem was suspected. An examination of the literature brought to light the work of Shartsis, et al[14] who measured surface tension in several binary silicate and borate systems. The estimated surface tension for glasses B, C, and H, based on their data, is given in Table II. The three glasses each show increasing surface tension with increasing temperature.[14] Though not large, this explains the contradictory results observed in the experiments using these glasses. This did not eliminate the possibility of other effects, but did indicate that the originally expected motion toward higher temperatures should not be observed.

The surface tension temperature coefficient of glass C in Table II is positive and about one-half the magnitude of borax (see next section). This still should have produced a readily observable bubble motion, but motion was only observed sporadically. This may be explained as follows. With a positive variation of tension with temperature, both thermal migration and buoyancy would act in the same direction causing bubbles to move upwards. This is what was observed. Bubbles rose, coalesced and were pinned at the surface, showing only halting movement at best. The combined buoyant and thermal gradient forces pinned bubbles to the top of the channel where any surface irregularities would interfere with lateral motion. Bubbles that did not finally work their way into the high gradient region drifted outward, but the motion

TABLE II

Calculated[+] Surface Tension for Lead Silicate and Borosilicate Glasses. Based on the Experimental Data of Shartsis, L., Spinner, S., and Smock, A. W., J. Research Natl. Bureau of Standards, 40, 61 (1948).

Glass (wt%)	Surface Tension (dynes/cm)				
	600°C	700°C	800°C	900°C	1000°C
B - 85 - PbO 7.5 - B_2O_3 7.5 - SiO_2	-	171.8	174.7	177.5	-
C - 85 - PbO 15 - SiO_2	-	182.5	187.3	192.4	194.6
H - 79 - PbO 11 - B_2O_3 8 - SiO_2 2 - Al_2O_3*	-	189.0	189.7	189.9	-
J - 73 - PbO 11 - B_2O_3 11 - Al_2O_3* 5 - SiO_2	-	-	-	-	-

[+]Additivity of surface tension for the PbO-SiO_2 and PbO-B_2O_3 systems is assumed.

*Effect of alumina in these systems is not known, therefore, no attempt was made to calculate values for glass J.

showed the effects of interference from the roof of the channel. This system could only be studied effectively in a low G environment.

3.2 Thermal Migration of Bubbles in Borax Glass

Thermal migration of bubbles in molten borax was observed in both a quartz capillary tube and with the inverted channel technique. The best observations were made with the inverted channel because its shallow depth (500 μm) allowed all bubbles to be seen at once and because there was good thermal contact with the heating strip, as discussed previously.

The thermal migration experiments were performed using the prototype hot stage. It was placed on the stage of a Zeiss Ultraphot III-B microscope. The heating strip was illuminated with the microscope lighting system and viewed in reflected light using a 4X objective lens, giving a total magnification of 50X. The working distance of the objective lens allowed the quartz cover of the hot stage to remain in place, as required for good temperature stability of the heating strip.

The inverted channel was filled using another technique. Bubble-containing glass rods were hand drawn from a crucible melt of borax. Rods of about 1 mm diameter were produced. A section of this rod ∿2.5 cm long was set on the cold heating strip. The quartz window containing the inverted channel was placed on top of the rod so that the rod was in the channel. The system was heated to completely melt the borax glass which then flowed wetting the quartz and filling the channel and the narrow seam between the rest of the quartz window and the platinum heating strip. The final equilibrium condition is illustrated in Fig. 3.

The bubbles, particularly in the hottest section, moved and coalesced during (mechanical) physical equilibration of the system. This resulted in a few larger bubbles in the center of the hot zone; but

in general, most of the bubbles in the cooler section did not have time to move very far in the first 1 to 2 minutes. The system was considered to be in mechanical equilibrium when bubbles trapped between the platinum heating strip and the quartz window (not in the channel) stopped moving. At this point several photographic sequences were taken with time intervals of 5 or 10 seconds in the sections with rapidly moving bubbles, and 20 seconds in the outer region with slower moving bubbles. It was noted that the bubbles trapped between the platinum and the quartz window (outside of the channel) showed little or no movement. Bubbles in the channel generally moved up the thermal gradient as was expected.

The bubble migration observed is well illustrated by Fig. 6. Here bubbles next to the channel wall (dark band just above two larger bubbles) are shown migrating toward a region of higher temperature. Two features to look for in this series of pictures are: 1) the acceleration as the bubbles move to higher temperature, and 2) larger bubbles move faster than smaller ones. The curved line defined by the bubbles in the series of eight pictures is due to acceleration. The difference in velocity due to size is illustrated by the second largest bubble overtaking the smaller one just ahead (to the right) of it, by the 20-second frame. Of significant importance is an apparent attraction of bubbles to one another, enhancing coalescence. This phenomena has not been reported before.

3.3 Comparison of Experiment with Existing Theory

The motion of an isolated bubble in a liquid with constant properties is given by the approximate formula of Young, Goldstein and Block (1959):

$$v_b \triangleq -D/4\eta \quad d\gamma/d\chi \qquad (4)$$

where v_b = velocity of the bubble
D = diameter of the bubble
η = viscosity of the liquid (melt), and
$d\gamma/d\chi$ = surface tension gradient.

(See Appendix D.)

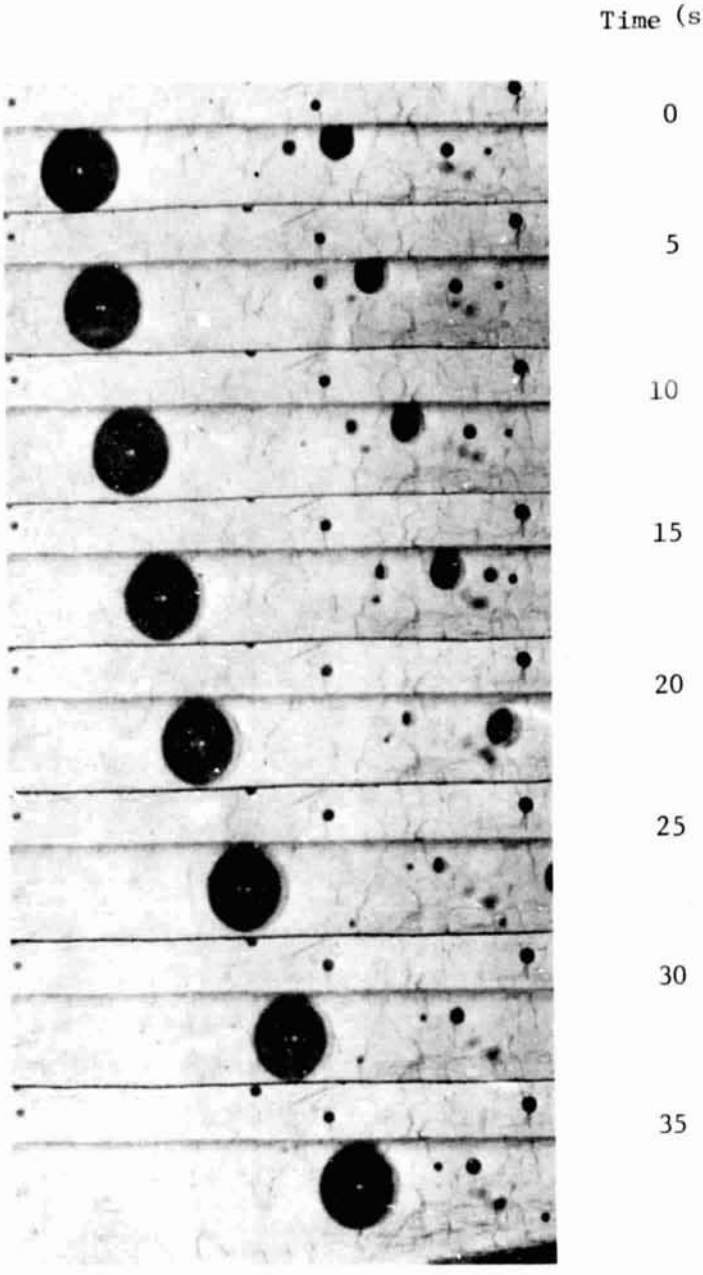

Fig. 6 - Bubble migration in a thermal gradient in molten borax. Large bubble has a diameter of 260 μm. Note bubbles accelerating as they move to higher temperatures.

In Fig. 7 a series of curves were plotted which correspond to the dependence of v_b on the bubble diameter, D, for a sequence of temperatures. Values of the viscosity, η, were interpolated from the reported values of Shartsis et al[15] for the Na_2O-B_2O_3 system. Their data (two points) were fit with the curve $\log \eta = 10.221 - 12153/T(°C)$. The surface tension gradient, $d\gamma/d\chi$, was calculated from the data of Shartsis and Capps[16] giving $d\gamma/dT = -.076$ dynes/cm-°C and a reasonable estimate of $dT/d\chi$ of 300°C/cm, giving $d\gamma/d\chi = -22.8$ dynes/cm^2. The data points plotted in the figure are bubble velocities determined from photograph sequences such as the one shown in Fig. 6. Three sequences were taken at approximately the same gradient and temperature conditions in different experiments. The data agree with the prediction that bubble velocity is proportional to bubble diameter. The dashed line shown in Fig. 7 is a visual fit to the observed bubble velocity-diameter trend. Using the velocity equation, a temperature of 785°C is estimated to have been the temperature at which these bubble velocities were measured. Data points for bubble velocities in a cooler section of the channel indicate a temperature at or below 700°C, which again is consistent with the temperature estimated for that region.

There are several conditions that might account for the scatter of the data points:

- There was a steep vertical gradient present as well as a horizontal gradient. Therefore small bubbles on the bottom saw the highest average temperature, and would have moved most rapidly.

- The vertical size of the channel was $\sim$500 μm. Large bubbles (<250 μm), therefore, were always within one radius of a boundary where any interaction would have slowed them down.

- There was some indication that bubbles tended to stick to the walls.

Curve 690119-A

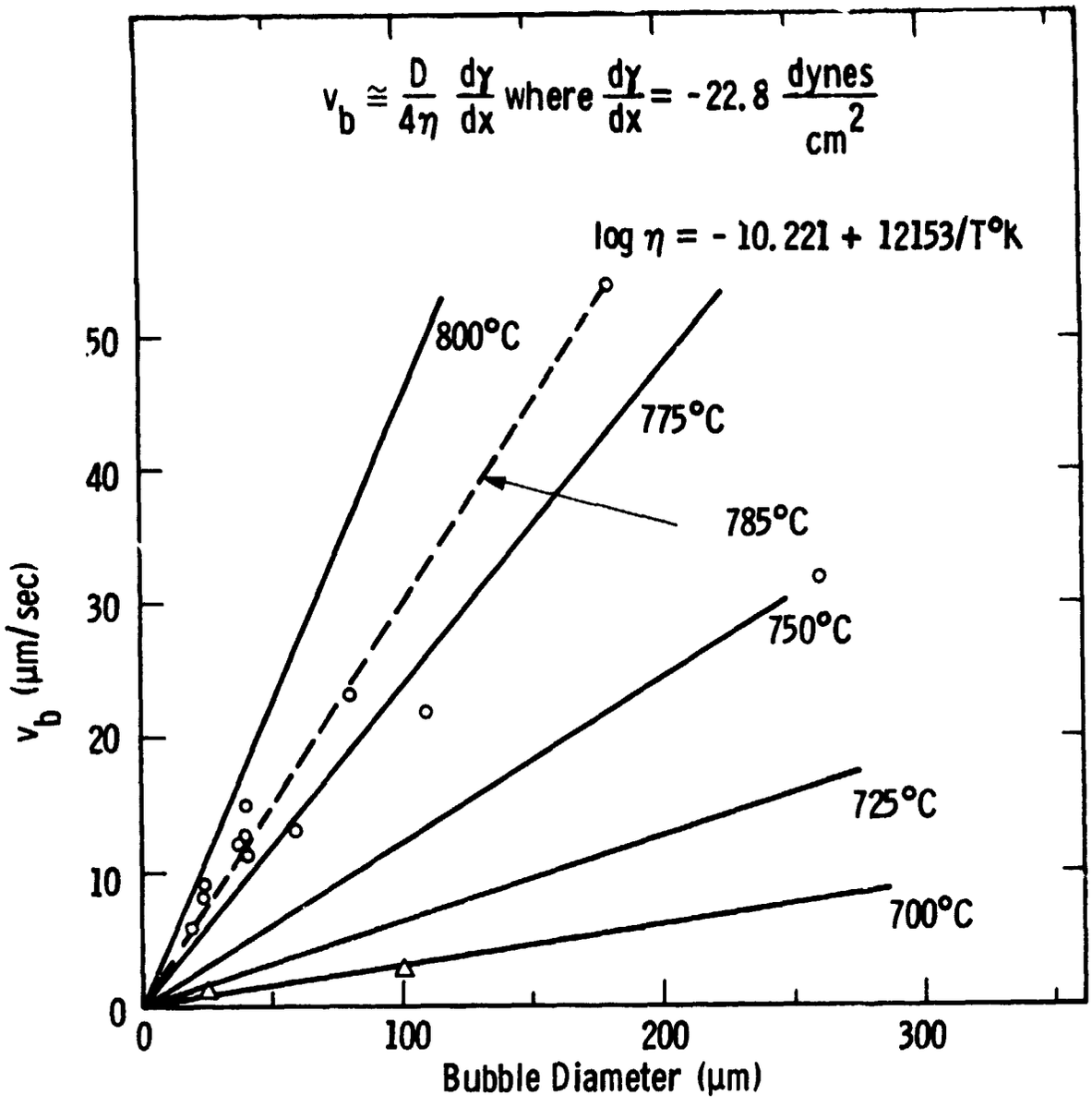

Fig. 7 – Comparison of predicted and measured bubble movement rates in molten borax.

o – measurements at high T near center of Pt strip

Δ – measurements at low T

Solid lines calculated from approximate equation assuming dT/dX = 300°C/cm. Dashed line drawn to fit high T data, with T ≈ 785, °C estimated by interpolation

- Bubbles apparently attracted each other, at least part of the time, so that bubbles separated by a distance less than about a diameter tended to interfere with each other. This was noted in measuring bubble velocities. Large ones appeared to drag smaller bubbles or even cause them to reverse their motion.

- Buoyant forces acted on the bubbles.

The fact that all the bubbles were not at the top of the channel in these experiments was probably due to the strong vertical gradient driving the bubbles down as in the experiments of Young, et al.[8] If $d\gamma/dt$ were not as large as it is for borax, or of opposite sign, the bubbles would all have been at the top of the channel.

3.4 Approximate Comparison of Thermal Gradient and Buoyant Forces in Molten Glass

The velocity of bubbles rising in a molten glass due to buoyancy is approximately $|V| = \frac{D^2 g\rho}{12\eta}$. Deviation from Stokes formula is due to nonrigidity of the bubbles. The velocity of a bubble due to a thermal gradient given previously is $|v| = D/4\eta \ \ d\gamma/d\chi$. Equating these velocities (equivalent to equating the forces) gives

$$D_{(cm)} = \frac{3 \ d\gamma/dT \ dT/d\chi}{g\rho} \qquad (5)$$

$$\cong .0001 \ \ dT/d\chi \ (°C/cm) \text{ for borax}$$

where $d\gamma/dT = .076$ dynes/cm-°C

$\rho = 2.4$ grams/cm^3.

In other words a bubble 300 μm in diameter in molten borax would not rise in a vertical downward thermal gradient of 300°C/cm. Smaller bubbles would move downward. This type of phenomena was observed in the experiments using molten borax.

4. SIGNIFICANCE OF RESULTS

For the first time in molten glass, the migration of bubbles driven by a thermal gradient has been observed. This mechanism, while perhaps commonly known in other systems, has not been identified as fundamental to glass processing technology in any of the current and classic texts. The results of this work show that for bubbles 300 μm and smaller and for thermal gradients which can reasonably be expected in sealing, enamelling and glass encapsulation (100-300°C/cm) that thermal fining dominates buoyant fining.

Even at this preliminary stage, these observations have implications which bear on the techniques of sealing, enamelling, encapsulation and passivation. They point to the need to generate the largest thermal gradients through the bubble-containing glass thicknesses as can be tolerated by the rigid components. The long-standing approach of substituting time-at-temperature for peak temperature excursion can only be beneficial to specimens oriented so as to be benefitted by buoyant fining.

Composition is seen to be a critical factor in the magnitude of the surface tension force. It has been seen that in the commercially very important $PbO-B_2O_3-SiO_2$ system, a striking dependency of the surface tension temperature coefficient is to be found. Slight alterations in the $PbO-B_2O_3$ ratio swing this coefficient from negative to positive through zero.[16] The substitution of SiO_2 for the B_2O_3 seems to drive the coefficient positive. These effects can have significant implication on the design of passivating glasses. Undoubtedly in the past, trial-and-error has led to the effective optimization of compositions to maximize thermal fining in many commercial sealing and enamelling systems, without a conscious

knowledge of this effect. With a firmer understanding of composition's role on surface tension coefficient, better designs could be produced more quickly.

The evidence of these experiments provides a high level of confidence that bubble migration in thermal gradients (thermal fining) is sufficient to serve as a method for the elimination of bubbles in glasses prepared in space. As pointed out, with reasonable gradients, bubbles could be driven out at rates comparable to those achieved on earth with buoyant forces. In order to apply this technique in the space environment, a much better understanding of the process must be obtained. This has been impossible under gravitational constraints. The difficulties are elaborated in Section 5.

5. NEED AND JUSTIFICATION FOR LOW-G EXPERIMENTS

We have demonstrated that a temperature gradient can cause bubbles to move in a temperature gradient, due to the dependence of surface tension on temperature. However, for several reasons it is impossible to do glass fining experiments on earth which are free of the effects of gravity. Most obvious is buoyancy-driven natural convection, which can cause rapid global movement of the glass melt and irregular thermal losses from the apparatus. Free convection in the melt can be avoided by use of a vertical geometry, taking care to avoid horizontal temperature gradients. Convective heat losses in the surroundings could be avoided by operating in a vacuum, for example. The other gravity induced problems outlined below can only be avoided by performing the experiments in space.

If a single bubble is used in a vertical apparatus, then bubble movement rates can be measured. However, because of buoyancy of the bubble, the movement rate will be quite different than in space. Nevertheless, such ground-based experiments can be used to test approximate theoretical results. For example this has been done by Young et al. to test their theoretical result, in which it was assumed that the movement rate was zero, i.e., the temperature gradient was adjusted so as to exactly compensate for buoyancy.

In glass fining we have the added complication that many bubbles are present, with a variety of sizes. Thus with gravity they will all rise at different rates, with the large ones overtaking the small ones. In addition, as we have observed experimentally, the bubbles seem to be attracted to one another in a temperature gradient. Such behavior can only be studied unequivocably in space.

5.1 Theoretical Work Needed in Support of Rocket Results

As noted earlier, the theory of Young et al[8] incorporates several assumptions:

- A single bubble in a large volume of liquid.
- Very low movement rates (actually $v_B \to 0$).
- Constant properties.
- No volatile components.

None of these assumptions are valid for glass ining. Merely doing experiments is insufficient to establish quantitative methods for proper design of space processing of molten glasses. New theoretical work is absolutely essential. In order of increasing difficulty this theoretical work should treat:

1. Finite movement rates without gravity.
2. Influence of variable properties, especially dependence of viscosity on temperature.
3. Influence of volatile component.
4. Interaction of bubbles with one another and with bounding surfaces of melt.

6. PROPOSED ROCKET EXPERIMENTS

Three rocket flights are proposed. The purpose of the flights are to obtain data in the absence of gravitational interference which will permit refinement and confirmation of the theoretical model for thermal fining in glasses. These experiments must encompass variations in surface tension, surface tension temperature coefficient, temperature, temperature gradient and volatility to develop an adequate theoretical model.

6.1 Glass Systems

Two glass compositions are proposed for evaluation. The first is the Borax glass, sodium tetraborate, and the second is a $PbO-SiO_2$ glass identified as glass C in Table I. The first glass is probably typical of most glasses in that it has a negative surface tension temperature coefficient. Two experiments are proposed with this glass. Bubble array motion would be studied with temperature gradients targeted at 100 and 300°C/cm, at an average temperature of approximately 780°C. The bubble arrays afford the advantage of being able to record data from a large number of bubbles of different sizes. This has the obvious advantage of improving the statistics of the data collection. In addition, apparent bubble interactions can be observed and these effects analyzed.

The third experiment will study the motion of bubble arrays in the $PbO-SiO_2$ glass in an intermediate temperature gradient (approx. 200°C). This system has a positive surface tension temperature coefficient causing bubbles to move to the colder end of the melt.

Where the precision of new theory dictates, measurements of surface tension and viscosity versus temperature will have to be made.

6.2 Data Treatment

6.2.1 Theoretical Model

Theoretical work will be carried out by Clarkson College personnel to derive an improved model over Young, et al[8] which will attempt to treat variable viscosity temperature properties, bubble interactions and component volatility.

6.2.2 Data Analysis

All of the photographic data will be converted to double notched 16 mm film and analyzed on the Clarkson College motion analyzer, by Clarkson personnel. This will permit accurate measurement of bubble position on each frame and automatic recording on computer cards. Telemetered temperature data will be converted to temperature gradients vs time. Results will be compared with the new theories.

6.3 Flight Hardware

6.3.1 Hot Stage

The hot stage will be one of two designs. Primary consideration will be given to reinforcing the design of the successful strip heater which uses the inverted channel and quartz cover slide (Fig. 1). A thicker platinum strip will be used to minimize the deformation around the thermocouple connections. In order to reduce temperature gradients through the thickness of the channel the back surface of the cover glass will be coated with an IR reflecting film of doped tin oxide. This is sufficiently transparent at these temperatures not to interfere with the optical measurements, yet it is thermally stable and an efficient IR reflector. The shape of the strip will be designed as in the past, but actual temperature profiles will be measured with welded thermocouples.

An alternative design will be briefly and initially considered. This design will simply consist of a small diameter fused quartz tubes with two independent heating coils attached to each end (Fig. 8). A doped tin oxide film would also be used on the outer surface of this tube in the gradient region to reduce transverse temperature gradients. The operation of this arrangement would be somewhat different in that both ends would first be heated simultaneously to the same temperature (the cold temperature), and then one end would be heated to the hot temperature to establish the gradient. The one thing that needs to be established in a simple preliminary earth-based experiment is to see that the equilibrium gradient can be established before all bubbles have migrated to one end. If this is the case, this simple design will replace the strip heater. Flight times may require treating transient gradients. Since multiple tubes can be used, data on several systems can be obtained in each flight.

6.3.2 Camera Requirement

Ideally photographs would be taken at a rate of one frame/s or greater. Continuous tungsten illumination has proven adequate.

6.3.3 Microscope

Simple, low power reflected light microscopy has proven to be sufficient in the ground based experiments. Either the reflectivity of the strip heater or the bubbles themselves has produced adequate contrast for good photographic coverage. Enhancement techniques such as polarized light and Nomarski phase contrast techniques did not prove necessary. Magnification of 20 to 40X would be ideal.

6.3.4 Controls

Necessary controls and power conditioning for the illumination and hot stage will have to be designed and constructed. Choice of techniques will be dictated by vehicle requirements.

Dwg. 6413A64

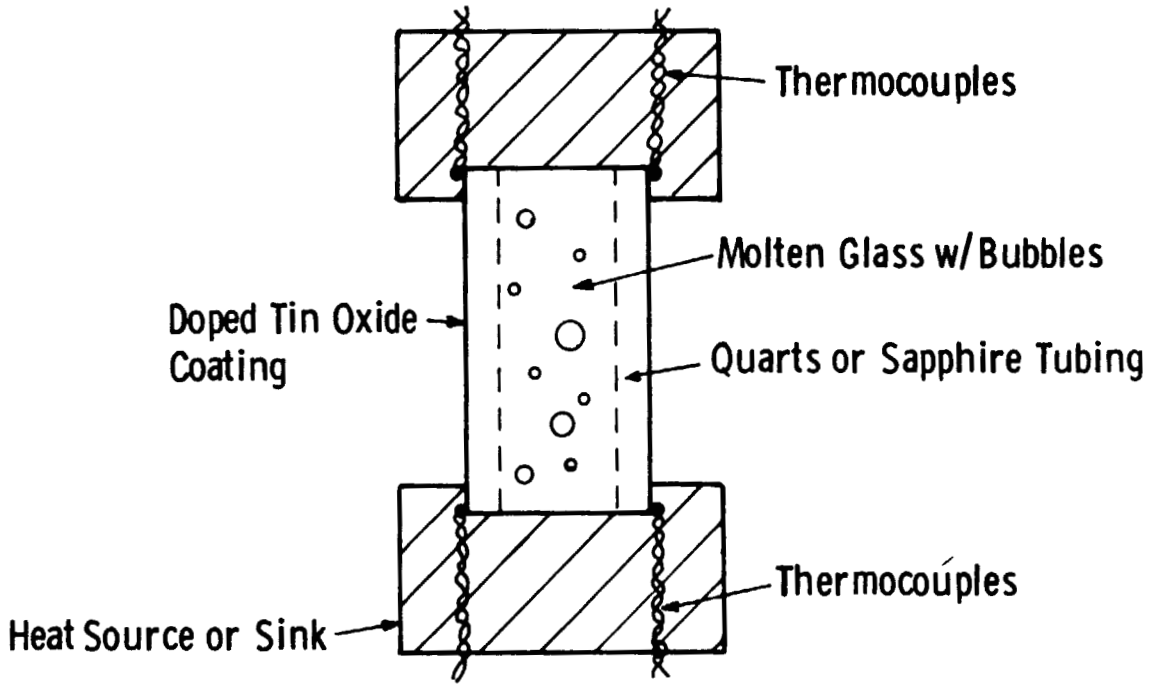

Fig. 8 – Alternate cell design for bubble migration experiment. Linear gradient through the cell achieved by controlling the temperature in the end caps. Thermocouples at each doped tin end of the cell used to control power to end caps. Oxide film reduces heat loss through the surface of the cell while allowing good optical observation

6.3.5 Testing

The system components will be tested to assure proper operation individually and as an integrated system under normal ground based conditions. Although the system will be designed to meet the anticipated flight environment, flight qualification testing will have to be negotiated.

6.3.6 Integration

The system will require a NASA-furnished multiple exposure camera and electrical power at 28 V (nom.) dc. Power requirements would fall in the range of 100 to 500 W, depending on the choice of illumination and hot stage control design. Camera interface requirements, power/heat dissipation constraints, and envelope limitations are required from NASA in the early phases of the equipment design programs.

6.4 Expected Results

6.4.1 Short Term

As a result of the proposed experiments, new and reliable theoretical models should be obtained for bubble migration due to thermal gradients in a molten glass. These formalisms should prove to be of great and wide-spread interest to the community of glass technologists. The implication of these findings should be felt in the design of glass compositions for semiconductor passivation, encapsulation, glass solder sealing, enamelling, and direct electric melting.

6.4.2 Long Term

The theoretical treatment of bubble migration in glasses due to thermal gradients would serve as the foundation for the adaptation of this mechanism to the fining of glasses, ceramics and metals manufactured in space. Melting techniques, post heating techniques and equipment will be designed, based on these results, which will be able to generate the indicated thermal gradients to fine space-melted materials. This will prove to be a powerful adjunct technique to the basic complement of space processing equipment.

REFERENCES

1. G. E. Rindone, Fining, Part I, Glass Industry, 38 (9) 1957 pg. 489-528.

2. G. E. Rindone, Fining, Part II, Glass Industry, 38 (10) 1957, pg. 561-577.

3. S. R. Scholes, Modern Glass Practice, Cahness Books, Boston, Mass., 1975, pg. 216.

4. C. H. Greene and R. F. Gaffney, Apparatus for Measuring the Rate of Absorption of a Bubble in Glass, J. Am. Ceram. Soc. 42(6) 1959, pg. 273.

5. R. H. Doremus, Diffusion of Oxygen from Contracting Bubbles in Molten Glass, J. Am. Ceram. Soc. 43 (12) 1960 p. 655.

6. M. Cable, A. R. Clarke, M. A. Haroon, Glass Tech. 9 (1968) p. 101; 10(1969) p. 15.

7. C. H. Greene and A. Haynes, Jr., Effect of As_2O_3 and $NaNO_3$ on the Solution of O_2 in Soda-Lime Glass, J. Am. Ceram. Soc., 48 (10) 1965 p. 528.

8. N. O. Young, J. S. Goldstein, and M. J. Block, "The Motion of Bubbles in a Vertical Temperature Gradient," J. Fluid Mech. 6, 350 (1959).

9. E. Roedder, 1965 Meeting of the Geological Society of America (from U.S. Geological Survey).

10. W. R. Wilcox, "Anomalous Gas-Liquid Inclusion Movement," Ind. Eng. Chem. 61, 76 (March 1969).

11. T. R. Anthony and H. E. Cline, "The Thermomigration of Biphase Vapor-Liquid Droplets in Solids," Acta. Met. 20, 247 (1972).

12. S. R. Coriell, S. C. Hardy and M. R. Cordes, "Melt Shape in Weightless Crystal Growth," NBSIR 77-1208, Feb. 1977.

13. Ibid., p. 75.

14. L. Shartsis, S. Spinner, and A. W. Smock, "Surface Tension of Compositions in the Systems $PbO-B_2O_3$ and $PbO-SiO_2$," J. Research Natl. Bureau of Standards, 40, 61, (1948).

15. L. Shartsis, W. Capps and S. Spinner, "Viscosity and Electrical Resistivity of Molten Alkali Borates," J. Am. Chem. Soc. 36, 319 (1953).

16. L. Shartsis and W. Capps, "Surface Tension of Molten Alkali Borates," J. Am. Ceram. Soc. 35, 169, (1952).

17. J.R.A. Pearson, J. Fluid Mech., 4, 489 (1958).

18. D. A. Nield, J. Fluid Mech. 19, 341 (1964).

19. H. J. Palmer and J. C. Berg, J. Fluid Mech. 47, 779 (1971).

20. Lord Rayleigh, Scientific Paper, Vol. 6, p. 432, Cambridge University Press, 1916.

APPENDIX A

Design of the Heating Strip for Glass Fining Experiments

The purpose of this exercise is to design the shape of the Pt-10/Rh heating strip so that a desired temperature gradient may be produced along its length. In keeping with the spirit of simplicity in these preliminary calculations, several assumptions will be made -- these may be justified on intuitive grounds and also supported by rough numerical calculations.

1. Steady state conditions will be assumed.

2. Under these conditions, the principal heat transfer out of the strip occurs by radiation from the bottom surface of the heating strip. There will be a certain amount of heat lost through the molten glass from the top and sides. However, an attempt to take this into account will lead to modeling which would be too complex to undertake at this stage and may not be worth the return. (Probably, this will be our weakest assumption.) There will also be heat lost by radiation from the sides of the platinum strip which, for similar reasons, will be ignored.

3. The bottom surface of the heating strip will be assumed to be a perfect black body. This may be achieved approximately by coating it with platinum black.

4. Temperature variations over the thickness of the heating strip will be ignored -- it can be shown that such variations should not be more than a fraction of a degree celsius.

It may be seen from the physics of the problem that the heating strip should be symmetric about the X-axis. The design question is "What is $y_1(x)$ so that $\frac{\partial T}{\partial x} = g$ where g is a specified constant?" Under the assumption of negligible temperature variations in the z-direction (normal to the plane of the paper), the differential energy balance for the heating strip takes the following form:

$$\nabla \cdot k\nabla T - \frac{1}{b}\sigma T^4 + \frac{I^2\rho(T)}{4b^2y_1^2} = 0 \qquad (1)$$

The symbols are defined below:

∇ = Two-dimensional gradient operator

T = Temperature in the strip in Kelvin

$T = T(x,y)$

b = Thickness of strip, cm

σ = Stefan-Boltzmann Constant

$\sigma = 5.67 \times 10^{-12} \ \frac{W}{cm^2K^4}$

I = Current through the strip, amps (it has been assumed here that the current distribution in the y-direction is uniform; this is not strictly true, but is a good approximation for small $y_1'(x)$. The level of approximation introduced by this assumption is probably consistent with that of the rest of the calculations, as will be seen later).

ρ = Specific resistivity of material of strip; ohm-cm. $\rho = \rho(T)$

k = Thermal conductivity of material of strip; $\frac{W}{cm-K}$

For the physical problem under consideration, one may write the following set of boundary conditions.

$$T(o,y) = T_1 \qquad (2)$$

$$T(L,y) = T_2 \qquad (3)$$

$$\frac{\partial T}{\partial y}(x,o) = 0 \qquad (4)$$

$$\nabla T \cdot \vec{n} = 0 \quad \text{on} \quad y = y_1(x) \qquad (5)$$

Where $\vec{n}$ is the normal to the curve $y = y_1(x)$.

Equation (5) may be rewritten as

$$-\frac{\partial T}{\partial x} y_1'(x) + \frac{\partial T}{\partial y} = 0 \text{ on } y = y_1(x) \tag{6}$$

Normally, $y_1(x)$ is specified and the problem for $T(x,y)$ is completely posed and may, in principle, be solved. However, here we wish to determine $y_1(x)$ given the requirement that

$$T(x,y) \sim T_1 + H(y)x \tag{7}$$

It is quite possible that no solution of the form of equation (7) exists for equations (1) thru (6). Anyway, let us introduce it into equation (1) and examine the result. Since it is known that the thermal conductivity of Pt - 10% Rh is practically constant over the temperature range of interest, the result is

$$kxH'' - \frac{1}{b}\sigma (T_1 + Hx)^4 + \frac{I^2\rho}{4b^2y_1^2} = 0 \tag{8}$$

It is clear from equation (8) that a solution of the form of equation (7) is <u>not suitable</u> unless H is a very weak function of y. In this case, equation (8) may be satisfied by the <u>approximations</u>

$$\frac{1}{b} (T_1 + \bar{H}x)^4 \approx \frac{I^2\rho}{4b^2y_1^2} \tag{9a}$$

$$H'' \approx 0 \tag{9b}$$

where $\bar{H}$ is a transverse average of H(y). In effect, equation (9a) strikes a balance between electrical dissipation and radiation from the surface ignoring conduction in the x-direction (which is being taken into account because of the change in cross-sectional area). Does equation (9b) have a meaningful solution? Since $H'(o) = 0$, the only solution is

$$H = \text{constant} \tag{10}$$

The boundary condition at $y = y_1(x)$ gives

$$-H|_{y=y_1} y_1'(x) + H'|_{y=y_1} x = 0 \tag{11}$$

with H = constant, this can be satisfied only if $y_1'(x) \approx o$.

What we have learned from the above is that a linear axial temperature gradient can be achieved only approximately. The approximation would

become better for smaller y_1'. So, our best hope is to use equation (9a) (which could have been obtained from a simple one-dimensional energy balance assuming no dependence of T on y) to obtain the required shape $y_1(x)$ and examine $y_1(x)$. The result is

$$y_1^2(x) = \frac{I^2\rho}{4b\sigma T^4} . \tag{12}$$

For a linear temperature gradient, we may write

$$T = T_1 + (T_2 - T_1)\frac{x}{L} \tag{13}$$

or $$\theta = T/T_1 = 1 + \alpha X \tag{14}$$

where $X = \frac{x}{L}$ and $\alpha = \frac{T_2-T_1}{T_1}$. If it is assumed that the specific resistivity ρ is linear in temperature over the range of temperatures involved,

$$\rho \sim \rho_1 + \frac{\rho_2-\rho_1}{T_2-T_1}(T-T_1) = \rho_1 + (\rho_2-\rho_1)\frac{x}{L} \tag{15}$$

or $$\psi = \rho/\rho_1 = 1 + \beta X \tag{16}$$

where $\beta = \frac{\rho_2-\rho_1}{\rho_1}$. [Here $\rho_1=\rho(T_1)$ and $\rho_2=\rho(T_2)$]

Defining $Y = \frac{y}{L}$ so that $Y_1(X) = \frac{y_1(x)}{L}$, we get

$$Y_1^2(X) = \left[\frac{I^2\rho_1}{4bL^2\sigma T_1^4}\right]\left\{\frac{1+\beta X}{(1+\alpha X)^4}\right\}$$

Since $y_1'(x) \equiv Y_1'(X)$, all we need to do is to perform a sample calculation with representative parameters to judge the degree of approximation made here. The following values are chosen as typical for the parameters.

$$\left.\begin{array}{l} T_1 \simeq (450°C) = 723°K \\ T_2 \simeq (550°C) = 823°K \end{array}\right| \rho_{0°C} \simeq 22.45\ \mu\Omega$$

$$\rho(T_1) = \rho_1 = 1.725\,\rho(t = 0°C) = 3.87 \times 10^{-5}\ \Omega\text{-cm}$$

$$\rho(T_2) = \rho_2 = 1.88\ \rho(t = 0°C) = 4.22 \times 10^{-5}\ \Omega\text{-cm}$$

$$\alpha = \frac{T_2 - T_1}{T_1} \simeq \frac{100}{723} = 0.138$$

$$\beta = \frac{\rho_2 - \rho_1}{\rho_1} \simeq \frac{(4.22 - 3.87) \times 10^{-5}}{3.87 \times 10^{-5}} = 0.09$$

$$L \simeq 1\ \text{cm}$$

$$b \simeq 2\ \text{mils} \simeq 5 \times 10^{-3}\ \text{cm}$$

$$\sigma = 5.67 \times 10^{-12}\ \frac{W}{cm^2 K^4}$$

$$I \simeq 8\ \text{amps}$$

we here
$$Y_1(X) = A^{1/2}\ \frac{(1 + \beta X)^{1/2}}{(1 + \alpha X)^2} \tag{18}$$

and, from this,

$$Y_1'(X) = A^{1/2}\ \frac{\beta - 4\alpha - 3\alpha\beta X}{2(1+\alpha X)^3 (1+\beta X)^{1/2}} \tag{19}$$

Here, the dimensionless group A is given by

$$A = \frac{I^2 \rho_1}{4bL^2 \sigma T_1^4} \simeq 0.08 \text{ for the above values of the parameters.}$$

The table below gives values of Y_1 and $Y_1'(x)$ calculated at various X-values using the above results.

X	$Y_1(X)$	$Y_1'(X)$
0	0.283	-0.0653
0.1	0.276	-0.0629
0.2	0.270	-0.0606
0.3	0.264	-0.0585
0.4	0.259	-0.0564
0.5	0.253	-0.0544
0.6	0.248	-0.0526
0.7	0.243	-0.0508
0.8	0.238	-0.0491
0.9	0.233	-0.0474
1.0	0.228	-0.0459

The shape of the strip is plotted in Figure A1.

Even though the shape of the strip appears almost trapezoidal, it is important to adhere to the exact shape given by equation (18) instead of a rough trapezoidal design since the table reveals a 42% change in Y_1' (based on the smallest value). From the physics of the problem it may be seen that the strongest variation of temperature with the y-coordinate would occur near the edges $y = \pm y_1(x)$. Therefore, it is important to focus the microscope in a region in the center of the strip around the x-axis.

Dwg. 6413A63

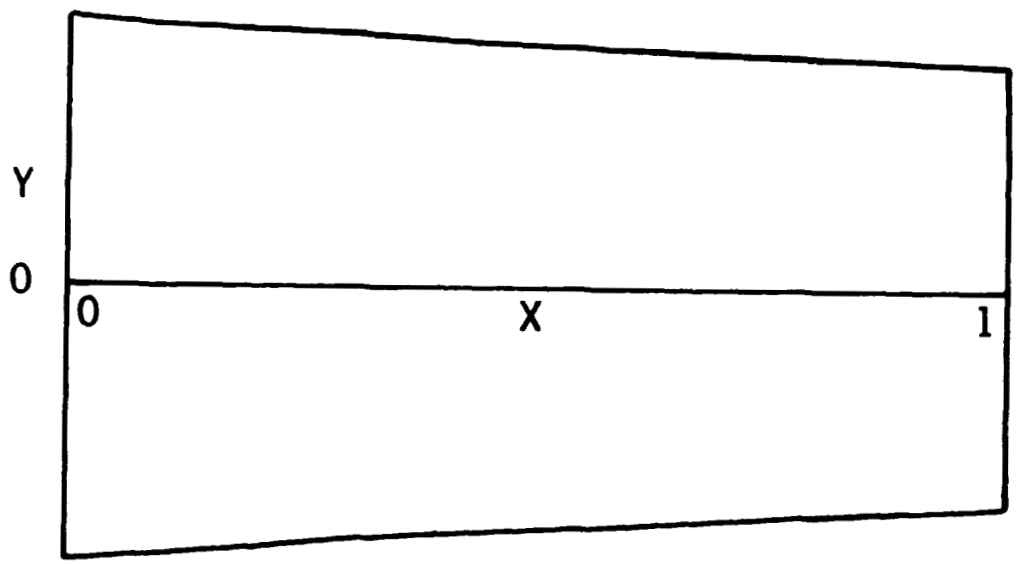

Fig. A1 – Sample design for Pt-10% Rh heating strip

ADDITIONAL ANALYSES OF TEMPERATURE VARIATION WITHIN THE STRIP

Temperature Variation Across the Thickness of the Strip

The maximum rate of heat loss from the strip due to radiation may be calculated as

$$q_r \sim \sigma T_2^4 \simeq 2.6 \frac{W}{cm^2}$$

An upper estimate of the temperature gradient in the z-direction may be obtained by assuming that all this energy is generated at the top surface of the strip and conducted through its thickness to the radiative surface. The normal conductivity of Pt-10% Rh is $\simeq 0.3 \frac{W}{cm\,°K}$ at 300°K(and is probably larger at a higher temp.) which gives a $\frac{\partial T}{\partial z} \simeq \frac{2.6 W/cm^2}{0.3 W/cm\,°K} = 9°K/cm.$

Since the thickness of the strip is 5×10^{-3}cm, the temperature variation across the strip is $\Delta T \simeq 0.05°K$ and may be safely ignored in this analysis.

Temperature Variation in the y-Direction

It appears that the temperature will decrease with distance from the x-axis in either direction so that the effect of temperature variation with the y-coordinate will be to force the bubbles to migrate towards the centerline. The maximum $\left|\frac{\partial T}{\partial y}\right|$ will occur at the boundaries $y = \pm y_1(x)$ and a rough estimate may be obtained from the boundary condition, equation (6).

$$\frac{\partial T}{\partial y} \simeq \frac{\partial T}{\partial x}\, y_1'(x)$$

$$\text{Max} \left| \frac{\frac{\partial T}{\partial y}}{\frac{\partial T}{\partial x}} \right| \simeq \text{Max} \left| y_1'(x) \right| = \text{Max} \left| Y_1'(X) \right| = 0.065$$

The actual ratio is probably smaller. In other words, the transverse temperature gradient will be much smaller than the axial temperature gradient. Such a gradient can probably be tolerated. It is important that the heat loss from the edges $y = \pm y_1(x)$ be held to a minimum since the effect of such loss

would be to increase $|\frac{\partial T}{\partial y}|$ and promote transverse variations in temperature. One way to accomplish this is to polish the edges to reduce radiation loss (which will be the principal means of heat loss in SPAR experiments).

Validity of the Assumption of Negligible Heat Loss From The Strip to the Glass Film

At steady state, with proper radiation shielding of the quartz cover on the glass film, there should be negligible radiation loss from the top surface of the quartz cover. So, the maximum heat loss from the strip to the glass film and quartz will probably be on the order of magnitude of the conduction rate in the glass film (and quartz) in the x-direction. Assuming an approximate gradient $\frac{\partial T}{\partial x} \sim 100 \frac{^{\circ}K}{cm}$, average thermal conductivity of 0.02 $\frac{W}{cm-^{\circ}K}$ for the glass film and the quartz cover, and a total cross sectional area for conduction $\leq 0.05\ cm^2$ (from glass film depth = quartz thickness = 0.025 cm and width $\leq$ 1 cm), the heat conduction rate in the x-direction is roughly

$$q \sim 0.02 \frac{W}{cm-^{\circ}K} \times 0.05\ cm^2 \times 100 \frac{^{\circ}K}{cm} = 0.1\ W$$

The heat lost from the bottom of the strip through radiation is

$$q_r \gtrsim 1.3\ W$$

assuming a minimum width of 1/2 cm for the strip. Thus, the heat loss by radiation will be the dominant factor balancing electrical dissipation in the strip.

APPENDIX B

Surface-Tension Driven Flow in the Molten Glass Film with a Free Surface

Assumptions

We shall make several reasonable assumptions in order to get a first estimate of the nature of the flow to be expected.

(1) Flow is assumed to be steady -- the fluid is bounded by suitable barriers at x=0 and L.

(1a) The length and width of the film are much larger than the depth. Therefore, variation in the z-direction can be ignored ($\partial/\partial z \equiv 0$), and away from x=0 and x=L, $\partial u/\partial x \approx 0$. Here, u is the x-component of the velocity field.

(2) Density variations with temperature will be ignored. Buoyancy driven convection may be ignored on earth as a first approximation. This is reasonable in view of the large surface to volume ratio in the film.

(3) Even though the surface will be deformed (for a balance of normal stresses), it will be assumed flat for convenience. The equation of continuity gives

$$\frac{\partial u}{\partial x} + \frac{\partial v}{\partial y} = 0 \rightarrow \frac{\partial v}{\partial y} = 0 \qquad (1)$$

Here v is the y-component of the velocity. Since v(0)=0, v=0 everywhere in our region of interest. Therefore, the variation of pressure in the y-direction is essentially hydrostatic and may be ignored for convenience. The principal variation of the pressure p will be in the x-direction under the assumptions, the only equation of motion that we need is the one for u. It simplifies to

$$\frac{\partial}{\partial y} \mu \frac{\partial u}{\partial y} = \frac{dp}{dx} \tag{2}$$

The boundary conditions on u(y) are:

$$\text{no slip at the wall} \qquad u(0) = 0 \tag{3}$$

$$\text{balance of tangential stresses at the surface} \qquad \left[\mu \frac{\partial u}{\partial y}\right]_{y=d} = \frac{d\gamma}{dx} \tag{4}$$

(Here γ is the surface tension.)

While μ will depend on y to a certain extent because of transverse temperature variations, its principal variation will be with x. So, it may be treated as a constant in the y-integration. The resulting velocity profile may be obtained by a straightforward integration of equation (2) to (4) to give

$$u(y) = \frac{1}{2\mu} \frac{dp}{dx} (y^2 - 2\,yd) + \frac{y}{\mu} \frac{d\gamma}{dx} \tag{5}$$

From the condition of no net flow at any axial location,

$$\int_0^d u\, dy = 0 \tag{6}$$

the pressure gradient may be related to the surface tension gradient. Using equation (5) in (6), the final result is

$$\frac{dp}{dx} = \frac{3}{2d}\frac{d\gamma}{dx} \tag{7}$$

This result may be used in equation (5) to rewrite the velocity field completely in terms of the surface tension gradient.

$$u(Y) = \frac{d}{4\mu}\frac{d\gamma}{dx}\ (3Y^2 - 2Y) \tag{8}$$

Here $Y = y/d$. The dimensionless velocity profile, U(Y) versus Y, is plotted in Figure 1

$$U(Y) = \frac{u}{(\frac{d}{4\mu}\frac{d\gamma}{dx})} = 3Y^2 - 2Y \tag{9}$$

It is clear from equation (9) [and the figure] that the maximum velocity (in magnitude) occurs at the surface Y=1. Its value is given by U=1. The velocity is zero at Y=2/3 and reaches a maximum in the negative X direction at Y=1/3, the magnitude being $|U| = 1/3$.

This means that

$$U_{max} = \frac{d}{4\mu}\frac{d\gamma}{dx} \tag{10}$$

and that the actual x-directional fluid velocity will change by 4/3 this amount across the depth of the film. It is interesting to compare the order of magnitude of these velocities with the velocities expected for the bubbles migrating in the temperature gradient. A first approximation to the bubble migration velocity may be obtained from the results of Young, et al (1959) as

$$v_{bubble} \approx -\frac{D}{4\mu}\frac{d\gamma}{dx} \tag{11}$$

Here, the variation of temperature with depth is ignored and γ, the interfacial tension between the liquid and the gas in the bubble, may be taken to be the same as the interfacial tension between the liquid

and the ambient medium. D is the bubble diameter. The negative sign indicates that the bubbles will migrate in the direction of the negative surface tension gradient (towards the hot end). Equations (10) and (11) imply serious consequences due to the surface-tension driven convection in the liquid film. It is seen from these equations that the bubble velocities will, in general, be smaller than or on the same order of magnitude as the fluid velocity. Furthermore, the fluid velocity changes substantially from the top of the film to the bottom (these regions are indistinguishable to the optical system since all depths are in focus). Not knowing the vertical position of a given bubble, it will be virtually impossible to extract its migration velocity in the temperature field by subtracting out the fluid motion. It should also be pointed out that for a film depth of 0.25 mm and a bubble diameter of 0.2 mm, even if we knew the vertical position of the center of the bubble, it will be hard to simply subtract out the motion of the fluid since the effect of large variations of the fluid velocity over the bubble dimensions is complex. Intuitively, such subtraction might be acceptable if the bubble dimensions are less than about a tenth of the film thickness. Under these conditions, of course, the convection in the film induced by surface tension variation will play a dominating role on bubble migration. The only acceptable solution seems to be to eliminate such convection thereby eliminating the free surface.

Example

A set of sample parameters are used below to calculate the expected order of magnitude of the velocities involved. Assume

$$d \approx 0.025 \text{ cm}$$

$$\mu \approx 10^2 \text{ poise (dynes sec/cm}^2\text{)}$$

$$\frac{d\gamma}{dT} \approx -0.06 \text{ dynes/cm °C}$$

$$\frac{dT}{dx} \approx -100 \text{ °C/cm}$$

Equation (10) gives the maximum velocity at the film surface as

$$U_{max} = \frac{d}{4\mu} \frac{d\gamma}{dx} = 3.75 \times 10^{-4} \text{ cm/sec}$$

For a bubble of diameter 0.005 cm, the migration velocity in the same temperature gradient, but in a stationary fluid, will be given by equation (11) as

$$|v_{bubble}| \approx \frac{D}{4\mu} \frac{d\gamma}{dx} = 0.75 \times 10^{-4} \text{ cm/sec}$$

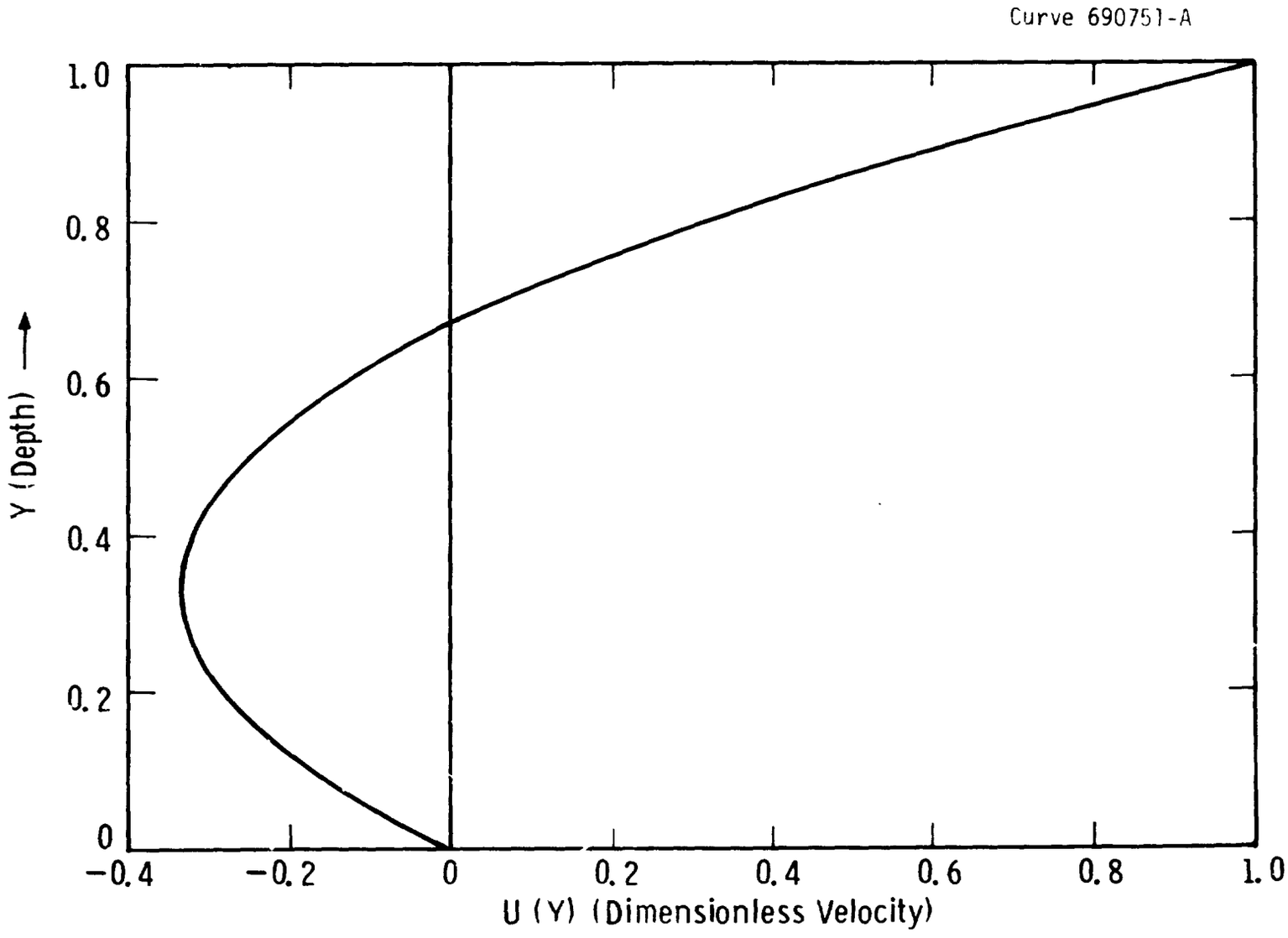

Fig. B1 – Dimensionless velocity in film as a function of depth

APPENDIX C

On the Stability of a Molten Glass Film Heating Uniformly From Below

It is desirable to make at least some rough preliminary estimates of the crucial stability parameters in the molten glass film. This is done below. (The two kinds of instabilities to be anticipated are: (1) Surface-tension driven cellular convection, (2) Buoyancy-driven cellular convection (only on ground).)

Marangoni Number

$$Ma = -\left(\frac{d\gamma}{dT}\right)\frac{D\Delta T}{\mu K} \qquad (1)$$

ΔT = Temperature difference across the film depth

$\frac{d\gamma}{dT}$ = Temp. gradient of surface tension

$\approx -0.06 \frac{\text{dynes}}{\text{cm } ^\circ\text{C}}$

D = Film depth = 0.025 cm

$\mu \approx 100$ poise $\left(\frac{\text{dyne sec}}{\text{cm}^2}\right)$

K = Thermal diffusivity of glass ≈ 0.01 cm^2/sec (rough estimate from Corning glass-properties booklet)

The above set of parameters will yield a conservative estimate for the Marangoni number. The result is

$$Ma \sim 0.0015\ \Delta T \qquad (2)$$

where ΔT is in °C. So, even for ΔT on the order of 100°C

$$Ma \approx 0.15 \qquad (3)$$

Now, for the onset of cellular convection driven by surface tension variations in the case of a liquid film heated by an isothermal surface, Pearson[17] gives

$$Ma_c \sim 80 \qquad (4)$$

(It should be noted here that the present discussion is not related to the surface-tension driven flow examined in Appendix B which is caused by axial temperature gradients. These can only be avoided by placing a slide over the melt. The present calculations are concerned with Benard-type cellular convection in the absence of any temperature gradients along the heating surface.) Even though our Marangoni number is much smaller than Ma_c from Pearson's analysis, it is important to look farther since Pearson completely ignored gravitational effects. Nield[18] showed that in the presence of gravity, buoyancy effects reinforce surface tension effects--that is, instability occurs at smaller critical values of the Marangoni number than those predicted by Pearson. Nield's analytical results received experimental verification a few years ago Palmer and Berg.[19] Therefore, it is important to also investigate the Rayleigh number which characterizes buoyancy effects.

Rayleigh Number (on ground)

$$Ra = \frac{g\alpha D^3 \Delta T}{K\,\nu} \qquad (5)$$

g : acceleration due to gravity = 980 cm/sec^2

D : film depth = 0.025 cm

K : thermal diffusivity of film $\approx$ 0.01 cm^2/sec

ν : kinematic viscosity

$$= \frac{\mu}{\rho} \approx \frac{100\ \frac{gm}{cm\cdot sec}}{3\ \frac{gm}{cm^3}} \approx 30\ cm^2/sec$$

α : thermal expansivity -- $\frac{\text{increase in volume}}{\text{volume x °C}}$

$\approx 10^{-4}$ (1/°C) Rough estimate

The result is

$$Ra \sim 5 \times 10^{-6} \Delta T \qquad (6)$$

Again, with $\Delta T = 100°C$,

$$Ra \sim 5 \times 10^{-4} \qquad (7)$$

which is extremely small compared to the critical Rayleigh Number Ra_c for the onset of buoyancy-driven convection calculated by Rayleigh.[20]

$$Ra_c \sim 1700 \qquad (8)$$

The conclusion, therefore, is that neither buoyancy-driven instability nor Marangoni instability should cause concern in the glass film. Again, this conclusion refers only to cellular convection.

APPENDIX D

Some Useful Information from Young et al[8]

The final result in Young et al contains some typographical errors and should read:

$$V_o = \frac{2}{3\mu(2\mu + 3\mu')} \left[\mu\gamma' RT_C - (\rho-\rho') gR^2 (\mu+\mu')\right] \qquad (9)$$

for dimensional consistency and for agreement with the Hadamard equation as $\gamma' \to 0$. However, when we tried to derive this result starting from Eq. (5) to (8) in Young, et al., we were unable to get exactly this result [or their Eq. (9)]. There appears to be a printing error in one or more of their starting equations.

Assuming, temporarily, that the above equation is correct, it is quite reasonable to let g = 0 in it for simulating zero gravity. So,

$$V_o = \frac{2\mu\gamma' RT_c}{3\mu(2\mu+3\mu')}$$

in Young et al. notation for this case. In view of some of the approximations made in arriving at this result, it is quite legitimate to make a few more → $\mu >> \mu'$; $h >> h'$. This gives

$$V = -\frac{1}{2}\frac{R}{\mu}\frac{\partial\gamma}{\partial z} \qquad (10)$$

Here:

V = velocity of bubble towards the hotter end

R = bubble radius

μ = viscosity of the continuous phase fluid

$\frac{\partial\gamma}{\partial z} = \frac{d\gamma}{dT}\frac{\partial T}{\partial z}$ ← Temp gradient in the continuous phase

↑

Rate of change of surface tension with temperature.